Stability and Thermodynamics of the $PtCl_2$ Type Catalyst for Activating Methane to Methanol: A Computational Study

Jeremy Kua,[†] Xin Xu,[†,‡] Roy A. Periana,[§] and William A. Goddard III*,[†]

Materials and Process Simulation Center, Beckman Institute (139-74), Division of Chemistry and Chemical Engineering, California Institute of Technology, Pasadena, California 91125, and Department of Chemistry, University of Southern California, Los Angeles, California 90089

Received March 2, 2001; Revised Manuscript Received November 8, 2001

Stimulated by the report of high-yield, low-temperature catalytic conversion of methane to methyl bisulfate (Periana et al., *Science* **1998**, *280*, 560), we studied the relative stability and reaction mechanism of the $Pt(NH_3)_2Cl_2$ and $Pt(bpym)Cl_2$ complexes in concentrated sulfuric acid. We find that the mechanism involves a series of steps beginning with C−H activation to form an intermediate ion-pair Pt(II)−CH_4 methane complex prior to forming a Pt(II)−CH_3 complex. Our calculated relative activation barriers for C−H activation are in good agreement with experimentally observed H/D ratios. Subsequent oxidation to a Pt(IV) complex can occur with reduction of SO_3. Release of methyl bisulfate regenerates the Pt(II) catalyst. Our calculations indicate that for the bipyrimidine system C−H activation prefers electrophilic substitution, whereas for the ammine system oxidation addition is more favorable. We find that the oxidation step (the rate-determining step) is more favorable for the ammine catalyst, suggesting higher activity than the bipyrimidine catalyst. However, we find that in sulfuric acid the ammine complex is unstable, while the bipyrimidine catalyst is stable. Bipyrimidine acts as a "proton sink", allowing the protonated form of the ligand to remain bound to Pt in concentrated sulfuric acid. These results are consistent with the observed behavior of the catalysts, suggesting that computational approaches may be useful in seeking modified catalysts that would be more economically feasible.

1. Introduction

The direct catalytic conversion of methane to methanol via a low-temperature route could provide an economic advantage over the current high-temperature processes involving the formation of syngas. The most promising route for low-temperature alkane activation has been the use of transition-metal complexes in solution, as indicated by the significant research activity in this area since the 1970s.[1−9] However, the low yields of new, low-temperature methane oxidation chemistries and/or high catalyst costs have prevented commercialization thus far. Methane is the most unreactive of the alkanes, and its oxidized products are typically more reactive, making selective oxidation a great challenge.

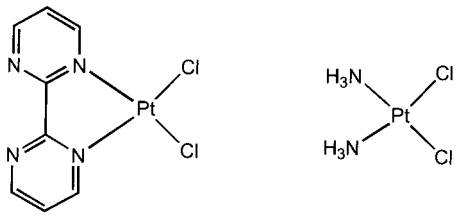

Figure 1. $(bpym)PtCl_2$ and $(NH_3)_2PtCl_2$ catalysts for methane activation.

The homogeneous catalysis of methane oxidation via C−H activation using platinum salts was first reported by Shilov et al.[10] Mercuric salts in concentrated sulfuric acid were shown by Periana et al., utilizing C−H activation chemistry, to produce a 43% one-pass yield.[11]

In 1998, Periana et al.[12] reported a significant breakthrough in developing an effective catalyst for high-yield selective oxidation of CH_4 to CH_3OH that allowed higher one-pass yields. This catalyst was formed from $PtCl_2$-(bpym) (Figure 1). In well-dried sulfuric acid (80 mL at 102%), they found that 72% of 115 mmol of CH_4 at 3.4

* To whom correspondence should be addressed. E-mail: wag@wag.caltech.edu.
† California Institute of Technology.
‡ On sabbatical leave from Xiamen University, China.
§ University of Southern California.

(1) Arnstden, B. A.; Bergman, R. G.; Mobley, T. A.; Peterson, T. H. *Acc. Chem. Res.* **1995**, *28*, 154.
(2) Bromberg, S. E.; Yang, H.; Asplund, C. M.; Lian, T.; McNamara, K. B.; Kotz, K. T.; Yeston, J. S.; Wilkens, M.; Frei, H.; Bergman, R. G.; Harris, C. B. *Science* **1997**, *278*, 260.
(3) *Selective Hydrocarbon Activation*; Davies, J. A., Watson, P. L., Liebman, J. L., Greenberg, A., Eds.; Wiley-VCH: New York, 1990.
(4) Hall, C.; Perutz, R. N. *Chem. Rev.* **1996**, *96*, 3125.
(5) Hill, C. L. *Activation and Functionalization of Alkanes*; Wiley-Interscience: New York, 1989.
(6) Sen, A. *Acc. Chem. Res.* **1988**, *21*, 421.
(7) Shilov, A. E.; Shul'pin, G. B. *Chem. Rev.* **1997**, *97*, 2879.
(8) Sommer, J.; Bukala, J. *Acc. Chem. Res.* **1993**, *26*, 370.
(9) Walktz, K. M.; Hartwig, J. F. *Science* **1997**, *277*, 211.
(10) Shilov, A. E. *Activation of Saturated Hydrocarbons by Transition Metal Complexes*; D. Riedel: Dordrecht, The Netherlands, 1984.
(11) Periana, R. A.; Taube, D. J.; Gamble, S.; Taube, H.; Satoh, T.; Fujii, H. *Science* **1998**, *280*, 560.
(12) Periana, R. A.; Taube, D. J.; Evitt, E. R.; Loffler, D. G.; Wentrcek, P. R.; Voss, G.; Masuda, T. *Science* **1993**, *259*, 340.

10.1021/om0101691 CCC: $22.00
Publication on Web 12/29/2001

MPa (~34 atm) was converted by 50 mmol of catalyst to product (mixture of $CH_3OSO_3H + CH_3OH$) in 2.5 h at 220 °C. They suggested that the reaction involved three processes:

$$\text{a. } CH_4 \text{ activation: } CH_4 + H_2SO_4 + SO_3 \rightarrow CH_3OSO_3H + H_2O + SO_2 \quad (1a)$$

$$\text{b. } CH_3OH \text{ conversion: } CH_3OSO_3H + H_2O \rightarrow CH_3OH + H_2SO_4 \quad (1b)$$

$$\text{c. S reoxidation: } SO_2 + {}^1/_2O_2 \rightarrow SO_3 \quad (1c)$$

leading to the net reaction

$$CH_4 + {}^1/_2O_2 \rightarrow CH_3OH \quad (2)$$

This process is very promising, since it provides high yield at relatively low temperatures. A potential industrial process involving continuous reoxidation and recycle of SO_2 using well-established sulfuric acid technology could be envisioned. However, due to the high costs of removal of water and methanol from concentrated sulfuric acid solvent and the severe inhibition of the catalyst by these materials, the process has not yet been commercialized.

Some experimental observations relevant to the mechanism of the bipyrimidine catalyst are as follows.

(i) Under conditions in which oxidized product is not made (<150 °C), H/D exchange is observed with CH_4 in D_2SO_4.

(ii) Addition of Pt(IV) salt as $H_2Pt(OH)_6$ to the catalyst results in the formation of product.

From these results, it is concluded that the C−H activation at 150 °C is via Pt(II) and the oxidation step is rate-determining.

Periana et al. found that the ammine catalyst $Pt(NH_3)_2Cl_2$ has higher initial activity than the bipyrimidine catalyst $Pt(bpym)Cl_2$. (The extrapolated turnover frequency (TOF) is on the order of 10^{-2} s^{-1}, an order of magnitude higher than for the bipyrimidine catalyst (TOF ≈ 10^{-3} s^{-1}).) However, after only several turnovers $PtCl_2$(solid) precipitated, halting the reaction ($\tau_{1/2} \approx 15$ min). In contrast, the bipyrimidine catalyst is stable over thousands of turnovers.

To provide a basis for improving these catalysts, we embarked on a project to elucidate the fundamental mechanism. The hope is that with an improved understanding of how the current catalyst works, we might be able to suggest possible modifications that could improve the catalyst sufficiently that it would become commercially viable.

Herein we report thermodynamics of many possible stable species and intermediates in solution. These calculations focus on the methane activation step (eq 1a) of the three processes in eq 1. Our calculated relative barriers for the C−H activation step with the bipyrimidine catalyst are in good agreement with observed ratios from H/D isotope exchange experiments. We find that C−H activation proceeds via electrophilic substitution for the bipyrimidine catalyst but via oxidative addition for the ammine catalyst. We also suggest mechanistic steps involved in oxidation and functionalization based on less complete calculations.

Section 2 presents details of the calculations, with the results addressing stability of the catalyst presented in section 3. Our results addressing methane activation are presented in section 4. This section is divided into three parts: mechanistic issues (section 4.1), the kinetics of C−H activation with $(bpym)PtCl_2$ (for which mechanistic experimental data are available) and $(NH_3)_2PtCl_2$ (section 4.2), and the overall thermodynamics of the reaction (section 4.3). A brief discussion follows in section 5 with concluding remarks in section 6.

2. Computational Details

All quantum-mechanical calculations were carried out using the B3LYP flavor of density functional theory (DFT). This includes nonlocal gradient corrections to the Slater local exchange functional[13] and includes exact Hartree−Fock (HF) exchange. We used the parameters referred to as Becke3[14] with the Becke nonlocal gradient correction,[15] the Vosko−Wilk−Nusair exchange functional,[16] and the Lee−Yang−Parr local and nonlocal correlation functional.[17]

The core electrons of the Pt were treated with a nonlocal ECP using angular momentum projection operators to enforce the Pauli principle.[18,19] To do this, we used the Hay and Wadt[20] core-valence effective core potential (ECP), which treats explicitly the outer 18 electrons of Pt (5s,5p,5d,6s,6p). This basis set is denoted as LACVP** in the Jaguar QM software.[21,22] H, C, and N atoms were treated at the level of 6-31G** (valence double-ζ plus polarization); while O and S were treated by 6-31+G* with diffuse functions being added.

All calculations used the Poisson−Boltzmann continuum approximation to describe the effect of solvent.[23−24] In this approximation, the solvent-accessible surface of the solute is calculated as illustrated in Figure 2 (using van der Waals radii for the atoms of solute and then rolling a sphere of radius R_{solv} of solvent over this surface to obtain a smooth surface). Then at each self-consistent-field (SCF) step, we calculated the reaction field in the solvent due to the electrostatic field of the solute wave function using the experimental dielectric constant ($\epsilon = 98$ for 99% H_2SO_4[25] and radius $R_{solv} = 2.205$ Å[26]). This reaction field was then included in the Fock operator (Kohn−Sham Hamiltonian) to calculate the orbitals of the DFT wave function of the solute. This calculation used a numerical grid to describe the solvent region of space. For a fixed geometry, this process was continued until self-consistent. The

(13) Slater, J. C. *Quantum Theory of Molecules and Solids*; McGraw-Hill: New York, 1974; Vol. 4 (The Self-Consistent Field for Molecules and Solids).
(14) Becke, A. D. *J. Chem. Phys.* **1993**, *98*, 5648.
(15) Becke, A. D. *Phys. Rev. A* **1988**, *38*, 3098.
(16) Vosko, S. H.; Wilk, L.; Nusair, M. *Can. J. Phys.* **1980**, *58*, 1200.
(17) Lee, C.; Yang, W.; Parr, R. G. *Phys. Rev. B* **1988**, *37*, 785.
(18) Goddard, W. A., III. *Phys. Rev.* **1968**, *174*, 659.
(19) Melius, C. F.; Olafson, B. O.; Goddard, W. A., III. *Chem. Phys. Lett.* **1974**, *28*, 457.
(20) Hay, P. J.; Wadt, W. R. *J. Phys. Chem.* **1985**, *82*, 299.
(21) Jaguar 3.5; Schrodinger, Inc., Portland, OR, 1998.
(22) Greeley, B. H.; Russo, T. V.; Mainz, D. T.; Friesner, R. A.; Langlois, J.-M.; Goddard, W. A., III; Honig, B. *J. Am. Chem. Soc.* **1994**, *116*, 11875.
(23) Tannor, D. J.; Marten, B.; Murphy, R.; Friesner, R. A.; Sitkoff, D.; Nicholls, A.; Ringnalda, M.; Goddard, W. A., III; Honig, B. *J. Am. Chem. Soc.* **1994**, *116*, 11875.
(24) Marten, B.; Kim, K.; Cortis, C.; Friesner, R. A.; Murphy, R. B.; Ringnalda, M. N.; Sitkoff, D.; Honig, B. *J. Phys. Chem.* **1996**, *100*, 11775.
(25) Klassen, J. K.; Fiehrer, K. M.; Nathanson, G. M. *J. Phys. Chem. B* **1997**, *101*, 9098.
(26) The probe radius is calculated from $r^3 = 3m\Delta/4\pi\rho$, where r is the solvent probe radius in Å, m is the molecular mass obtained by dividing the molecular weight given in ref 27 in by Avogadro's number (6.023×10^{23}), Δ is the packing density (assumed to be 0.5),) and ρ is the density given in g/cm^3 at 20 °C obtained from ref 27.
(27) Lide, D. R. *Handbook of Chemistry and Physics*, 74th ed.; CRC Press: Boca Raton, FL, 1993.

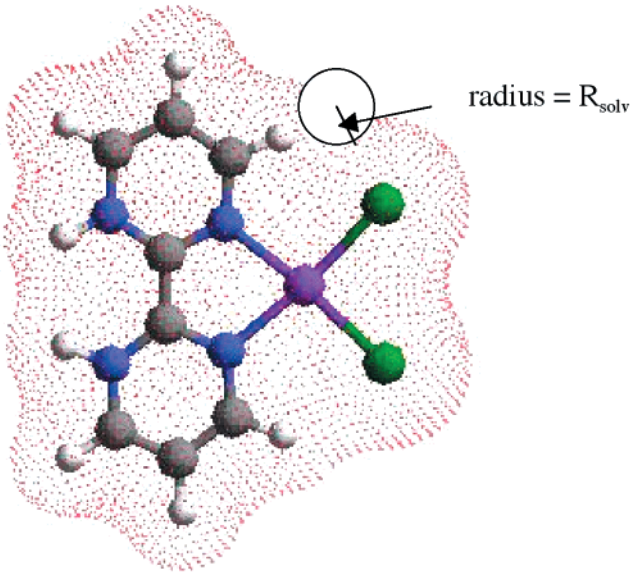

Figure 2. Illustration of the solvent-accessible surface used in the calculation of the Poisson−Boltzmann solvation energy.

total energy then included the QM energy (which includes rearrangement effects due to the solvent) and the solute−solvent interactions. The forces on the QM atoms due to the solvent are also calculated so that the geometry could be calculated in the presence of the solvent. However, in this work, the single-point solvation (free) energy was calculated at each optimized gas-phase geometry.

The analytical Hessian was calculated at each optimized geometry in the gas phase. The DFT gas-phase energy was corrected for the zero-point vibrations to obtain ΔH_{0K}. In addition, we used the vibrational frequencies to calculate the enthalpy and entropy as a function of temperature to obtain the total free energy ΔG_{TK} at finite temperature T. For the reaction energies (Table 3), we report two numbers.

(i) The first number, ΔH_{0K}, is the sum of the electronic energy, solvation energy, and zero-point energy with no temperature corrections. This corresponds to the enthalpy change at 0 K.

(ii) The second number, ΔG_{453K}, adds the free energy correction from 0 to 453 K to the ΔH_{0K} number. Note that we do *not* correct the free energy for concentration differentials among reacting species to obtain the chemical potential. Such concentration corrections can be significant, since some of the reactions studied include ligand exchange with the solvent (sulfuric acid) present in much higher concentration than the other species in solution.

The various discussions in the text will mainly be based on ΔG_{453K}.

3. Results on Catalyst Stability in Sulfuric Acid

3.1. Ammine Ligands. We calculate that in sulfuric acid the ammine ligands in $Pt(NH_3)_2Cl_2$ are favorably displaced by bisulfate ligands.

$$Pt(NH_3)_2Cl_2 + 2H_2SO_4 \rightarrow [Pt(OSO_3H)_2Cl_2]^{2-} + 2[NH_4]^+ \quad (3)$$

$$\Delta H_{0K} = -32.5 \text{ kcal/mol}, \Delta G_{453K} = -23.4 \text{ kcal/mol}$$

The driving force for this reaction is the favorable protonation of the ammine ligands to form NH_4^+, which goes into solution.

In fact, we find that at 453 K the bidentate form of bisulfate is the thermodynamically favored species.

$$[Pt(OSO_3H)_2Cl_2]^{2-} \rightarrow [Pt(\eta^2\text{-}OSO_3H)Cl_2]^- + [OSO_3H]^- \quad (4a)$$

$$\Delta H_{0K} = 15.6 \text{ kcal/mol}, \Delta G_{453K} = -5.7 \text{ kcal/mol}$$

The protonated form of bisulfate ligands is highly unfavorable.

$$[Pt(OSO_3H)_2Cl_2]^{2-} + 2H_2SO_4 \rightarrow [Pt(OSO_3H_2)_2Cl_2]^0 + 2[OSO_3H]^- \quad (4b)$$

$$\Delta H_{0K} = +31.9 \text{ kcal/mol}, \Delta G_{453K} = +30.0 \text{ kcal/mol}$$

Structures and relevant bond distances of these Pt complexes are shown in Figure 3b.

The favorable thermodynamics for decomposition of the ammine complex suggests that it may be short-lived, as observed. The loss of the ammine ligands is the first step of $PtCl_2$(solid) precipitation.

3.2. Bipyrimidine Ligand. For the bipyrimidine ligand, we consider three cases (unprotonated, singly protonated and doubly protonated). We find the following.

(i) The singly protonated form, $[Pt(bpymH)Cl_2]^+$ is the most stable.

(ii) ΔG_{453K} for forming the doubly protonated form, $[Pt(bpymH_2)Cl_2]^{2+}$, is only 4.9 kcal/mol higher in energy.

(iii) ΔG_{453K} for forming the neutral unprotonated form, $[Pt(bpym)Cl_2]$, is 7.8 kcal/mol less stable in solution (it is the most stable in the gas phase).

Thus

$$[Pt(bpym)Cl_2] + H_2SO_4 \rightarrow [Pt(bpymH)Cl_2]^+ + [OSO_3H]^- \quad (5a)$$

$$\Delta H_{0K} = -7.6 \text{ kcal/mol}, \Delta G_{453K} = -7.8 \text{ kcal/mol}$$

$$[Pt(bpymH)Cl_2]^+ + H_2SO_4 \rightarrow [Pt(bpymH_2)Cl_2]^{2+} + [OSO_3H]^- \quad (5b)$$

$$\Delta H_{0K} = +6.1 \text{ kcal/mol}, \Delta G_{453K} = +4.9 \text{ kcal/mol}$$

Our calculations suggest that the singly protonated form would be dominant in the real catalytic environment. However, the differently protonated forms are accessible to allow proton shuttling to facilitate the activation and oxidation steps (discussed in section 4.3.4).

The geometries of these complexes are given in Figure 3a. A somewhat surprising result from these calculations is that the structure of $[Pt(bpym)Cl_2]$ hardly changes upon adding the protons. Thus, the Pt−N bond distances increase slightly (0.005 Å) and the Pt−Cl bond distances decrease slightly (0.05 Å) upon protonation. The central C−C bond connecting the two pyrimidine units changes very little (from 1.48 to 1.45 Å). The pyrimidine groups in all three cases are parallel when-bound to the $PtCl_2$ complex.[28] Thus, the bipyrimidine ligand functions as a proton reservoir.

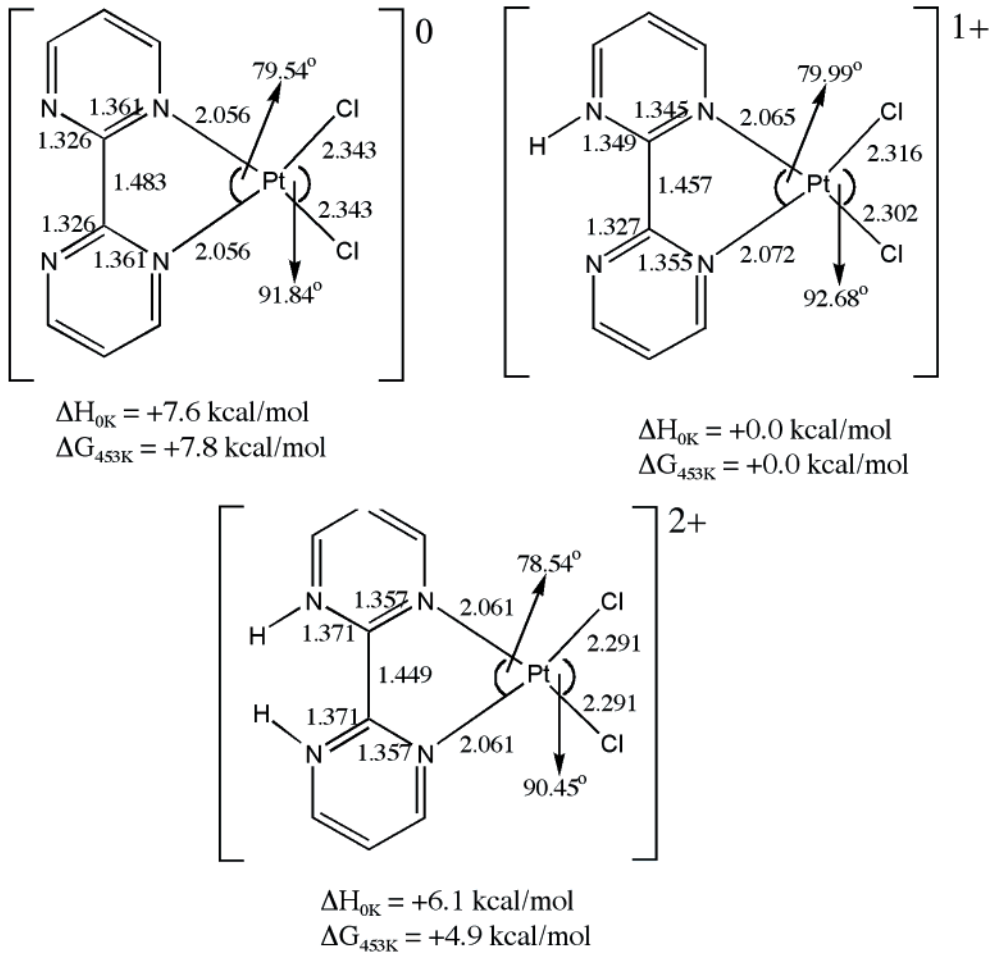

Figure 3. Geometries of different forms of the catalyst: (a, top) unprotonated and singly and doubly protonated forms of the bipyrimidine catalyst; (b, bottom) ammine and bisulfate forms of the catalyst. The small changes near the Pt indicate that little charge is removed from the Pt, while the small changes in the bpym ligand indicate that the charge is localized near the protons.

These bpym structures are more stable than the bisulfate systems. For example

$$[Pt(bpymH_2)Cl_2]^{2+} + 2[OSO_3H]^- \rightarrow [Pt(OSO_3H)_2Cl_2]^{2-} + [bpymH_2]^{2+} \quad (6)$$

$\Delta H_{0K} = +0.3$ kcal/mol, $\Delta G_{453K} = +18.4$ kcal/mol

This contrasts dramatically with the ammine case in eq 3.

(28) In free bipyrimidine the calculated angle between the pyrimidine planes was 28.4°. The energy required to twist the planes parallel was calculated to be −2.7 kcal/mol, including solvation and zero-point energy corrections.

Energies for the various species are reported in Table 1. The most stable form of free bipyrimidine in solution is the doubly protonated form. Adding the third proton is uphill: 8.5 kcal/mol. Thus, bipyrimidine retains two unprotonated N sites that can form a complex with $PtCl_2$ even in concentrated sulfuric acid.

4. Results for Conversion of CH_4 to CH_3OSO_3H

4.1. Mechanistic Issues. 4.1.1. Mechanism Proposed by Current Calculations. Our calculations support a reaction mechanism with three basic steps (see Figure 4a).

(i) With a square-planar Pt(II) complex as starting material, methane activation occurs via an intermediate

Table 1. Energetics of $L_2Pt_nCl_{2n}$ Complexes and Other Reacting Species

compd	electronic *E* (hartree)	solvation *E* (kcal/mol)	ZPE (kcal/mol)	$G_{0\rightarrow 453K}$ (kcal/mol)
$[(NH_3)_2PtCl_2]^0$	−1 152.799 824	−30.2	51.4	−38.0
$[(OSO_3H)_2PtCl_2]^{2-}$	−2 439.049 954	−160.3	37.4	−51.2
$[(\eta^2\text{-}OSO_3H)PtCl_2]^-$	−1 739.356 347	−55.6	18.6	−42.4
$[(H_2SO_4)_2PtCl_2]^0$	−2 440.066 346	−13.9	51.6	−51.7
$[(bpymH_2)PtCl_2]^{2+}$	−1 567.650 889	−221.5	103.1	−46.5
$[(bpymH)PtCl_2]^+$	−1 567.468 698	−80.0	95.8	−45.9
$[(bpym)PtCl_2]^0$	−1 567.127 652	−23.7	87.6	−46.4
$[NH_4]^+$	−56.904 893 53	−89.3	31.1	−18.0
$[bpymH_3]^{3+}$	−528.102 348 0	−417.2	108.3	−37.9
$[bpymH_2]^{2+}$	−528.068 820 5	−186.5	101.1	−37.1
$[bpymH]^+$	−527.835 306 8	−56.5	92.8	−37.0
bpym (bipyrimidine)	−527.449 428 2	−13.4	84.0	−37.6
H_2SO_4	−700.226 950 5	−14.3	24.0	−29.3
$[OSO_3H]^-$	−699.724 028 8	−67.7	16.4	−29.9
CH_4	−40.523 252 46	1.7	28.3	−18.1
HCl	−460.797 487 2	−0.8	4.2	−18.4
SO_3	−623.766 593 1	−5.4	7.3	−25.6
SO_2	−548.594 640 4	−4.3	4.2	−25.4
H_2O	−76.418 146 75	−6.8	13.3	−18.4
CH_3OSO_3H	−739.530 641 8	−10.6	41.8	−33.1

ion-pair methane complex, $[L_2Pt^{II}X(CH_4)]$, to produce a $CH_3-Pt(II)$ square-planar complex.

$$[L_2Pt^{II}Cl_2]^{m+} + CH_4 \rightarrow [L_2Pt^{II}Cl(CH_4)]^{(m+1)+}Cl^- \quad (7a)$$

$$[L_2Pt^{II}Cl(CH_4)]^{(m+1)+}Cl^- \rightarrow [L_2Pt^{II}Cl(CH_3)]^{m+} + HCl \quad (7b)$$

(ii) Oxidation of $CH_3-Pt(II)$ to an octahedral $CH_3-Pt(IV)$ complex can occur via adding bisulfate ligands in the axial positions with reduction of SO_3.

$$[L_2Pt^{II}Cl(CH_3)]^{m+} + 2H_2SO_4 + SO_3 \rightarrow [L_2Pt^{IV}Cl(CH_3)(OSO_3H)_2]^{m+} + SO_2 + H_2O \quad (8)$$

(iii) Functionalization occurs via reductive elimination of CH_3OSO_3H.

$$[L_2Pt^{IV}Cl(CH_3)(OSO_3H)_2]^{m+} \rightarrow [L_2Pt^{II}Cl(OSO_3H)]^{m+} + CH_3OSO_3H \quad (9)$$

After $[L_2Pt^{II}Cl(OSO_3H)]$ (eq 8) is formed from one turnover, the catalytic cycle can proceed using $[L_2Pt^{II}Cl(OSO_3H)]$ as the catalyst without further involving the $[L_2Pt^{II}Cl_2]$ species. Hence, eq 7a is replaced by eq 7a′ for subsequent catalytic cycles.

$$[L_2Pt^{II}Cl(OSO_3H)]^{m+} + CH_4 \rightarrow [L_2Pt^{II}Cl(CH_4)]^{(m+1)+} + OSO_3H^- \quad (7a')$$

This mechanism shares similarities with both the aqueous Pt(II)/Pt(IV) system proposed by Shilov[10,29−30] and the Periana mechanism[12] (Figure 4b) discussed below.

4.1.2. Comparison with Experiment. Periana et al. suggested that C−H activation takes place via electrophilic substitution, going through a dissociative step to form the 14-electron T-complex, $[(bpym)Pt^{II}Cl]^{m+}$ (see Figure 4b). Subsequent reaction with methane (eq 10b) leads to the $CH_3-Pt(II)$ intermediate.

$$[(bpym)Pt^{II}Cl_2]^{m+} \rightarrow [(bpym)Pt^{II}Cl]^{m+1}\cdots Cl^- \quad (10a)$$

$$[(bpym)Pt^{II}Cl]^{m+}\cdots Cl^- + CH_4 \rightarrow [(bpym)Pt^{II}Cl(CH_3)]^{m+} + HCl \quad (10b)$$

The Periana T-complex (eq 10a) is similar to the methane complex intermediate found in eq 7a. However, we find that as one Cl^- is removed, it is favorable for the CH_4 to occupy the open coordination site. Hence, our mechanism goes through a methane complex intermediate rather than the T-complex.

Neither the 14-electron T-complex nor the methane complex have been directly observed experimentally. However, should such intermediate species be formed, conversion to the $CH_3-Pt(II)$ species (eqs 7b and 10b) is calculated to be exothermic, probably making it short-lived.

The most significant mechanistic information comes from H/D exchange experiments with D_2SO_4 at temper-

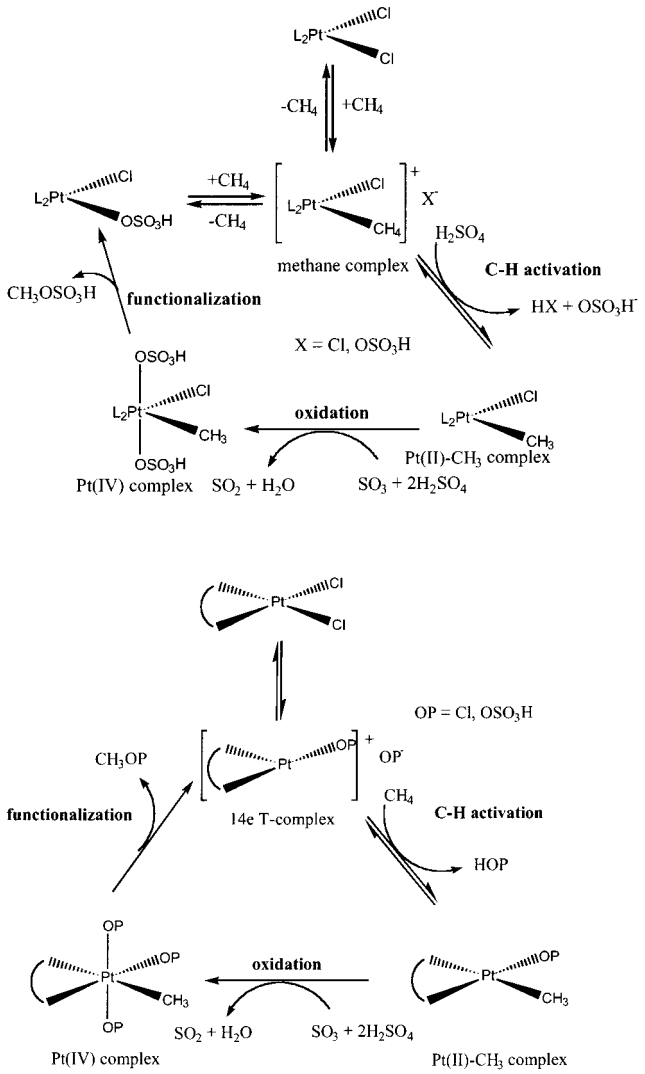

Figure 4. Overall mechanism of catalytic cycle: (a, top) as suggested from the calculations; (b, bottom) as proposed originally by Periana et al.

(29) Siegbahn, P. E. M.; Crabtree, R. H. *J. Am. Chem. Soc.* **1996**, *118*, 4442.
(30) Holtcamp, M. W.; Labinger, J. A.; Bercaw, J. E. *J. Am. Chem. Soc.* **1997**, *119*, 848.

atures below 150 °C (where no oxidized products are made). Here significant amounts of highly deuterated species (CD_4, CD_3H, and CD_2H_2) are observed. This suggests that the activation barrier of the reverse reaction (eqs 7a and 10a) is higher than the forward reaction (eqs 7b and 10b).

The large excess of H_2SO_4 in solution favors the formation of HCl as Cl^- goes into solution.

$$H_2SO_4 + Cl^- \rightarrow HCl + OSO_3H^- \qquad (11)$$

The proposed oxidation (eq 8) and functionalization (eq 9) steps are consistent with our calculations.

4.1.3. Comparison with Previous Calculations. Hush and co-workers have reported calculations of the thermodynamics for the ammine complex.[31] They used the same level of DFT as our work. Also for the metal they used a similar level of calculations (but with the Stoll ECP[32,33] instead of the Hay and Wadt ECP). However, for the nonmetal atoms their calculations were less rigorous. Thus, in Hush's calculations, the core electrons of the C, N, S, O, and Cl atoms were replaced with simplified core potentials and they used only valence double-ζ basis sets (no polarization functions). In addition, no diffuse functions were used. In contrast, we found that diffuse functions for O and S are very important to properly describe the stabilization of the OSO_3H^- anion.

The treatment of solvation is also different. Hush et al. used the isodensity polarizable continuum model (IPCM).[34] We used the Poisson−Boltzmann continuum approximation, which has been thoroughly tested for solvation energies of many organics and metal-containing systems.

Hush found that for the ammine catalyst C−H activation via oxidative addition is *less* favorable compared to electrophilic substitution. In contrast, we find oxidative addition is more favorable than electrophilic substitution in the ammine system. They found that ligand exchange results in the *exchange of the two chlorides* with two bisulfate molecules (eq 12).

$$[(NH_3)_2PtCl_2] + 2H_2SO_4 \rightarrow [(NH_3)_2Pt(OSO_3H)_2] + 2HCl \qquad (12)$$

In contrast, we find this to be quite unfavorable (as discussed in section 4.3.3). The CH_3−Pt(II) complex then goes through similar oxidation and functionalization steps as proposed by Periana et al.[12]

Hush's calculations would lead to a net reaction free energy of −66.7 kcal/mol in solution at 298 K for the net reaction of methane activation

$$CH_4 + 2H_2SO_4 \rightarrow CH_3OSO_3H + 2H_2O + SO_2 \qquad (13)$$

while our calculations give −21.3 kcal/mol. This 45.4 kcal/mol energy difference results from differences both in the gas-phase calculations and in the thermal corrections. On the other hand, the solvation energy contributions from the two methods are similar for this case.

4.2. Calculated Kinetics of C−H Activation. 4.2.1. (bpym)$PtCl_2$. Figure 5 shows the C−H activation reaction energy profile (ΔH(0K)) in solution for (bpym)-$PtCl_2$.[35] We find a distinct stable intermediate **B**. Since the barrier for the reverse reaction **B** → **A** is larger than the forward barrier **B** → **C** and since subsequent reactions of **C** are not favorable (low temperature, <150 °C), we expect multiple exchanges with deuterium in D_2SO_4 before desorption of methane, as observed.

We calculate the overall reaction **A** → **C** to be endothermic by 19.6 kcal/mol. We find that the first step to C−H activation involves the breaking of one Pt−Cl bond. Methane occupies the open coordination site, forming the methane complex **B**. Cl^- remains very closely associated as an ion pair and can be involved in breaking the C−H bond to form **C**. The calculated barrier of **B** → **C** is small, 35.2 − 30.8 = 4.4 kcal/mol (going through transition state **T2**), which may explain why **B** is transient. We find that the reverse reaction **B** → **A** indeed has a larger barrier (40.7 − 30.8 = 9.9 kcal/mol).[36]

The direct reaction pathway from **B** to **C** via transition state **T2** corresponds to C−H activation via an electrophilic substitution mechanism. There is no formation of an intermediate species with a Pt−H bond. As the Pt−C bond is formed, the breaking of the C−H bond is assisted by the Cl^- of the ion pair. We also carried out calculations for the oxidative addition mechanism. Here both Pt−H and Pt−C bonds are formed as the C−H bond is broken. This leads to the intermediate **D** via transition state **T2b**. Elimination of HCl from **D** leads back to **C**. We find that the barrier from **B** to **C** via **T2** (35.2 − 30.8 = 4.4 kcal/mol) is 9.1 kcal/mol lower than from **B** to **D** via **T2b** (44.3 − 30.8 = 13.5 kcal/mol). This suggests that *C−H activation of methane via (bpym)$PtCl_2$ favors electrophilic substitution over oxidative addition*.

The highest barrier for the overall reaction **A** → **C** via electrophilic substitution is estimated to be 40.7 kcal/mol (**T1**). As discussed in section 4.1.1, after one turn of the catalytic cycle the initial species in solution, (bpym)$PtCl_2$, is converted into (bpym)Pt(Cl)(OSO_3H). We find that exchanging a Cl^- ligand for an OSO_3H^- ligand is endothermic (by ΔH(sol, 0 K) = 6.4 kcal/mol; ΔG(sol, 453 K) = 11.7 kcal/mol). Hence we expect the effective overall barrier, ΔH(sol, 0 K), to be less than 34 kcal/mol (since the Pt−O bond in Pt−OSO_3H is weaker than the Pt−Cl bond).[37] Similarly, the relative energetics, ΔH(sol, 0 K), of the analogous **B**, **T2**, **C**, **T2b**, and **D** with respect to (bpym)Pt(Cl)(OSO_3H), **A′**, are 24.4, 28.8, 13.2, 37.9, and 19.3 kcal/mol instead of 30.8, 35.2, 19.6, 44.3, and 25.7 kcal/mol, respectively.

(31) Mylavaganam, K.; Backsay, G. B.; Hush, N. S. *J. Am. Chem. Soc.* **1999**, *121*, 4633.

(32) Igel-Mann, G.; Stoll, H.; Preuss, H. *Mol. Phys.* **1988**, *65*, 1321.

(33) Andrae, D.; Haussermann, U.; Dolg, M.; Stoll, H.; Preuss, H. *Theor. Chim. Acta* **1990**, *77*, 123.

(34) Foresman, J. B.; Keith, T. A.; Wiberg, K. B.; Snoonian, J.; Frisch, M. J. *J. Phys. Chem.* **1996**, *100*, 16098.

(35) Note that in calculating the kinetics all species are included; i.e., we do not calculate reactant fragments as separated species at infinity.

(36) From our calculations on C−H activation barriers of small hydrocarbons on a Pt surface (Kua, J.; Goddard, W. A., III. Unpublished results), we find that DFT/B3LYP with the same basis set systematically overestimates barriers by ∼5 kcal/mol when compared to experiment. The numbers we report are the actual calculated numbers without any corrections.

(37) This estimate presumes the pathway for the bisulfate ligand is very similar to that for chloride. Calculations with the bisulfate ligand are currently in progress (Philipp, D.; Xu, X.; Goddard, W. A., III. Manuscript in preparation).

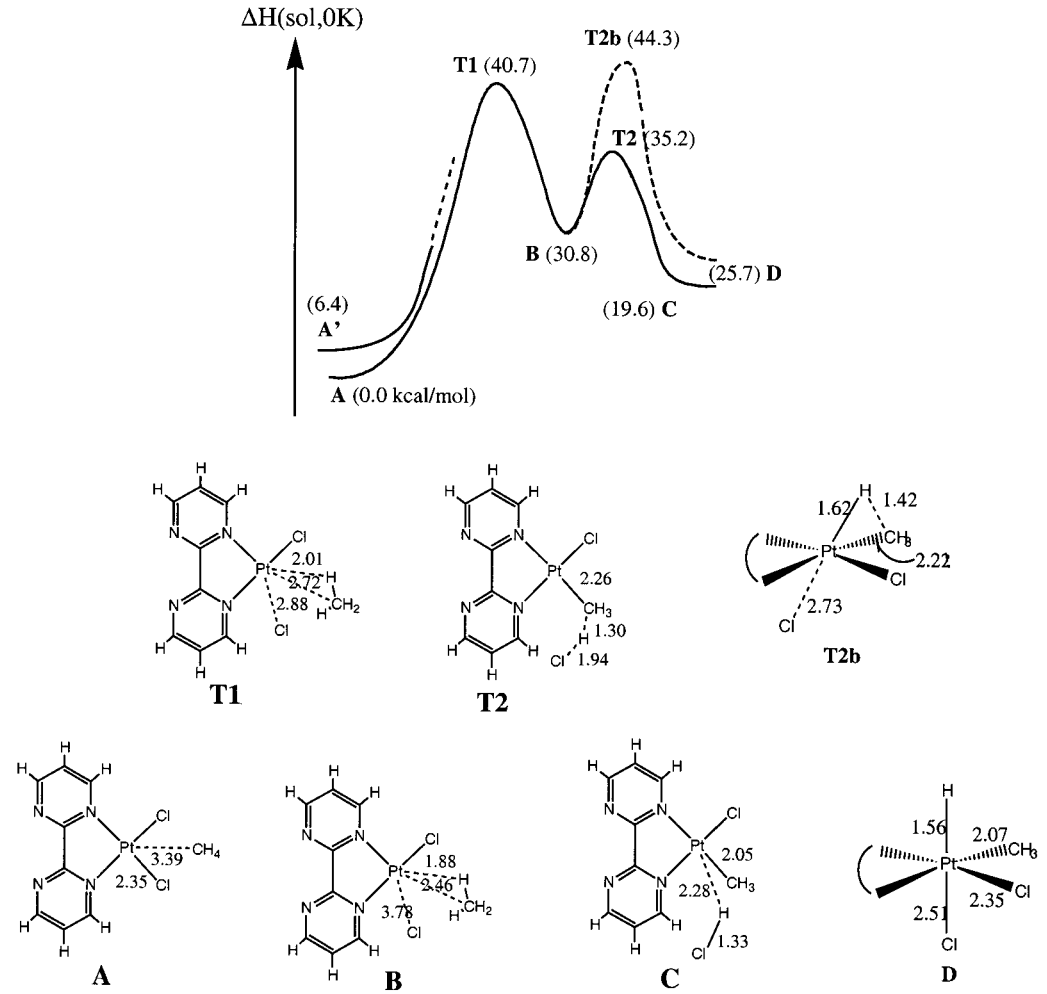

Figure 5. C−H activation reaction energy profile of (bpym)$PtCl_2$. The calculated structures for the stable intermediates (no negative eigenvalues in the Hessian) and the transition states (one negative eigenvalue in the Hessian) are also reported. The pathway **A** → **T1** → **B** → **T2** → **C** provides the lowest energy reaction path for activating CH_4. The barrier for **B** → **T2** → **C** (4.4 kcal/mol) versus **B** → **T2** → **A** (9.9 kcal/mol barrier) is consistent with the H/D exchange experiments. The pathway **B** → **T2** → **C** corresponds to electrophilic substitution, while **B** → **T2b** → **C** (13.5 kcal/mol barrier) corresponds to oxidative addition. **A′** shows the relative energy for (bpym)Pt(OSO_3H)Cl.

These results are consistent with experimental observations providing strong support of our mechanism for C−H activation, in particular, that an ion pair methane complex intermediate, **B**, is involved (as opposed to a single-step reaction).

4.2.2. $(NH_3)_2PtCl_2$. Because it is unstable in sulfuric acid, H/D exchange experimental data are not available for the ammine catalyst (it forms precipitate leading to catalyst death, as discussed in section 3). However, our calculations for the kinetics of C−H activation suggest that the ammine catalyst (if it were stable in solution) would have a different reaction profile compared to the bipyrimidine catalyst.

Figure 6 shows the reaction energy profile (ΔH(0 K) in solution) of $(NH_3)_2PtCl_2$. The overall reaction **A** → **C** is endothermic by 26.2 kcal/mol. Methane occupies the open coordination site, forming a distinct intermediate methane complex, **B**, 23.6 kcal/mol uphill from **A**. Cl^- remains very closely associated as an ion pair and is involved in breaking the C−H bond to form **C**. The relative barrier heights[36] are opposite to those found for (bpym)$PtCl_2$. The forward reaction **B** → **C** is 42.1 − 23.6 = 18.5 kcal/mol (going through transition state **T2**), while the reverse reaction **B** → **A** has a smaller barrier (33.1 − 23.6 = 9.5 kcal/mol).

We find that $(NH_3)_2PtCl_2$ favors oxidative addition over electrophilic substitution. The barrier for the reaction **B** → **D** via **T2b** is 32.1 − 23.6 = 8.5 kcal/mol. This is 10.0 kcal/mol lower than electrophilic substitution of **B** → **C** via **T2** (42.1 − 23.6 = 18.5 kcal/mol). This suggests that *direct C−H activation can involve either electrophilic substitution or oxidative addition depending upon the ligands.*

As discussed in section 4.1.1, after one turn of the catalytic cycle, the reacting species changes from $(NH_3)_2$-$PtCl_2$ to $(NH_3)_2Pt(Cl)(OSO_3H)$. We find that exchanging a Cl^- ligand for an OSO_3H^- ligand is endothermic (by ΔH(sol, 0 K) = 3.4; ΔG(sol, 453 K) = 6.7kcal/mol) leading to a first barrier (ΔH(sol, 0 K),**T1**) of 29.7 kcal/mol instead. Similarly, the relative energetics (ΔH(sol, 0 K)) of the analogous **B**, **T2**, **C**, **T2b**, and **D** with respect to $(NH_3)_2Pt(Cl)(OSO_3H)$ (**A′**) are 20.2, 38.7, 22.8, 28.7, and 18.0 kcal/mol instead of 23.6, 42.1, 26.2, 32.1, and 21.4 kcal/mol, respectively.

4.3 Calculated Thermodynamics for Conversion of CH_4 to CH_3OSO_3H. 4.3.1. Overall Thermodynam-

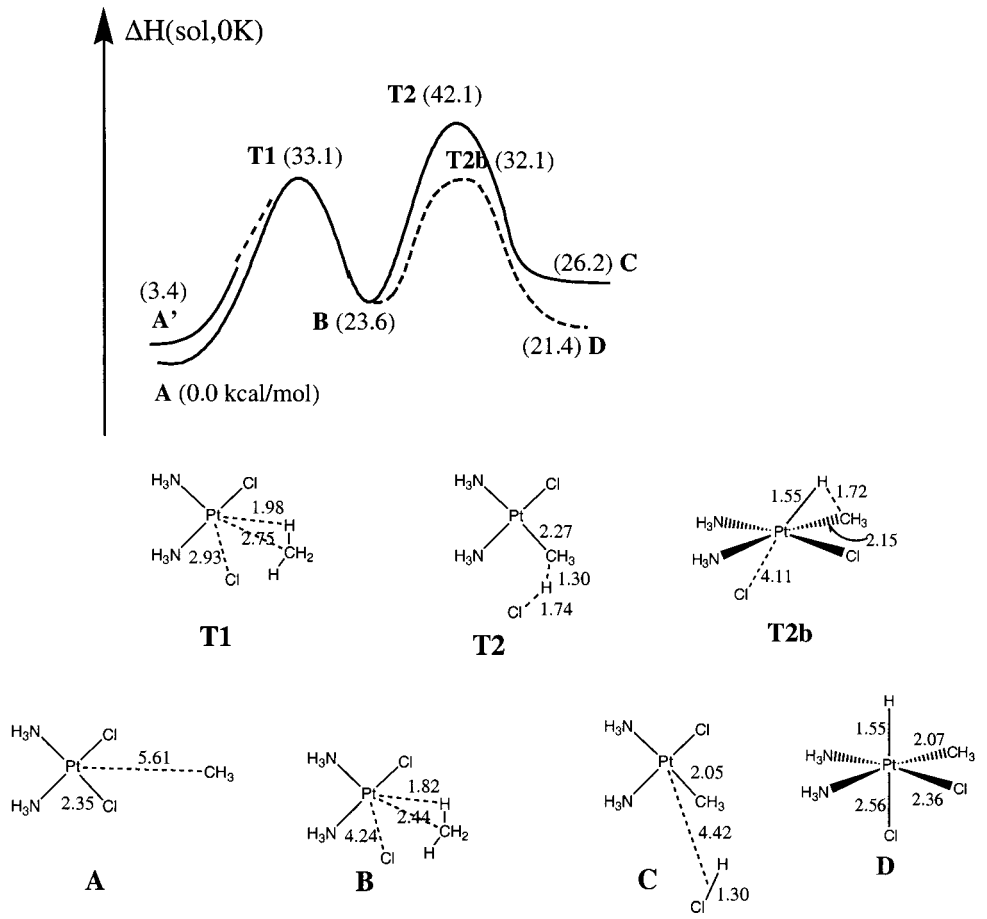

Figure 6. C−H activation reaction energy profile of $(NH_3)_2PtCl_2$. The pathway **A** → **T1** → **B** → **T2** → **C** provides the lowest energy reaction path for activating CH_4. The pathway **B** → **T2b** → **C** (8.5 kcal/mol) corresponds to oxidative addition, while **B** → **T2** → **C** (18.5 kcal/mol barrier) corresponds to electrophilic substitution. **A′** shows the relative energy for $(NH_3)_2Pt(OSO_3H)Cl$.

ics. The overall thermodynamics calculated for various steps in the conversion of CH_4 to CH_3OSO_3H are shown in Figures 7 and 8 for six different cases (L = NH_3, L = OSO_3H, L_2 = η^2-OSO_3H, L_2 = bpymH$_2$, L_2 = bpymH, L_2 = bpym). In this diagram, the starting point (L_2PtCl_2) is at the upper right and the species with Cl replaced by CH_3 is at the bottom right. The pathway to get here involves the stable intermediate $[L_2Pt(CH_4)Cl]^+$ at the far right. From the lower right we go up to the left to form the oxidized Pt(IV) complex with two $(OSO_3H)^-$ ligands. This involves several intermediate steps that we leave out in the diagram. From here reductive elimination leads to the CH_3OSO_3H product and the modified catalyst $L_2Pt(OSO_3H)Cl$ in the upper middle. Subsequently, this would be considered the catalyst. Thus, the first turnover involves the cycle at the far right, while subsequent ones go from $L_2Pt(OSO_3H)Cl$ to $[L_2Pt(CH_4)Cl]^+$.

From $L_2Pt(OSO_3H)Cl$, one can also consider a second cycle in which the Cl^- is lost while the $(OSO_3H)^-$ is retained. This catalytic cycle is shown at the lower right.

In addition, we examined a pathway where formation of the Pt−CH_3 bond occurs without displacing the Cl^- ligands. This is also represented by the left side of Figures 7 and 8, where L = Cl.

Energetics for the reaction intermediates are given in Table 2, while energy differences of the reactions (ΔH_{0K} and ΔG_{453K}) are given in Table 3. The alpha-numeric labels for each reaction are shown in Figure 7b. For convenience in comparing the two major types of ligands, we present the results for L = NH_3 and L_2 = bpymH in parts a and b of Figure 8. The reactions can be partitioned into three groups.

The first group involves the reactions in the top half of parts a and b of Figure 7 (reactions **6**−**9**). This describes the overall thermodynamics for ligand exchange between Cl^- and OSO_3H^- and determines the dominant forms of the catalyst in solution. Chloride from the complex goes into solution as HCl in fuming sulfuric acid.

The second group of reactions is the (lower right) catalytic cycle involving the L_2PtXCH_3 intermediates, where X = Cl. Formation of Pt(II)−CH_3 via C−H activation is given by reactions **10a** and **11a**. The oxidation step is reaction **3a**. The functionalization step is reaction **4a**. Reactions **1a** and **5a** form the methane complex (L_2PtXCH_4 species) as a stable intermediate, which leads to C−H activation via reaction **2a**. We expect the methane complex to be transient in this two-step C−H activation. It has not been detected directly by experiment. However, we calculate this complex to

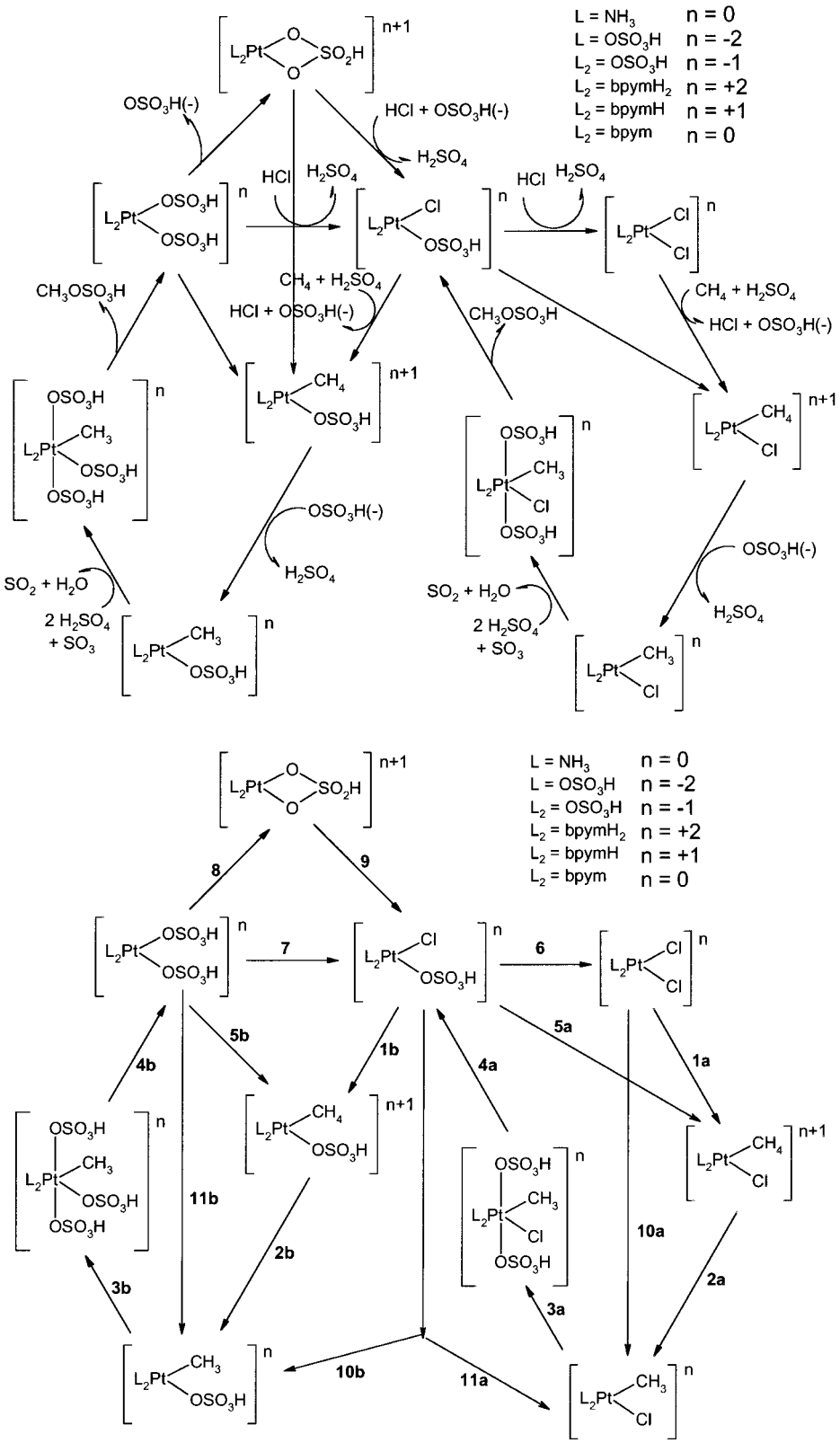

Figure 7. Calculated overall thermodynamics of the catalytic cycle: (a, top) chemical steps; (b, bottom) definitions for the energetics (in Table 3).

be stable and our interpretation of the isotope experiments involves the existence of this species.

The third group is the (lower left) catalytic cycle involving the L_2PtXCH_3 intermediates, where X = OSO_3H. Formation of Pt(II)−CH_3 via C−H activation is given by reactions **10b** and **11b**. The oxidation to form the Pt(IV) intermediate is reaction **3b**. The functionalization step is reaction **4b**. Reactions **1b** and **5b** form the stable methane complex (L_2PtXCH_4 species) as a stable intermediate, which leads to C−H activation via **2b**.

For C−H activation to occur in a single step requires simultaneous breaking of the C−H and Pt-X bonds with

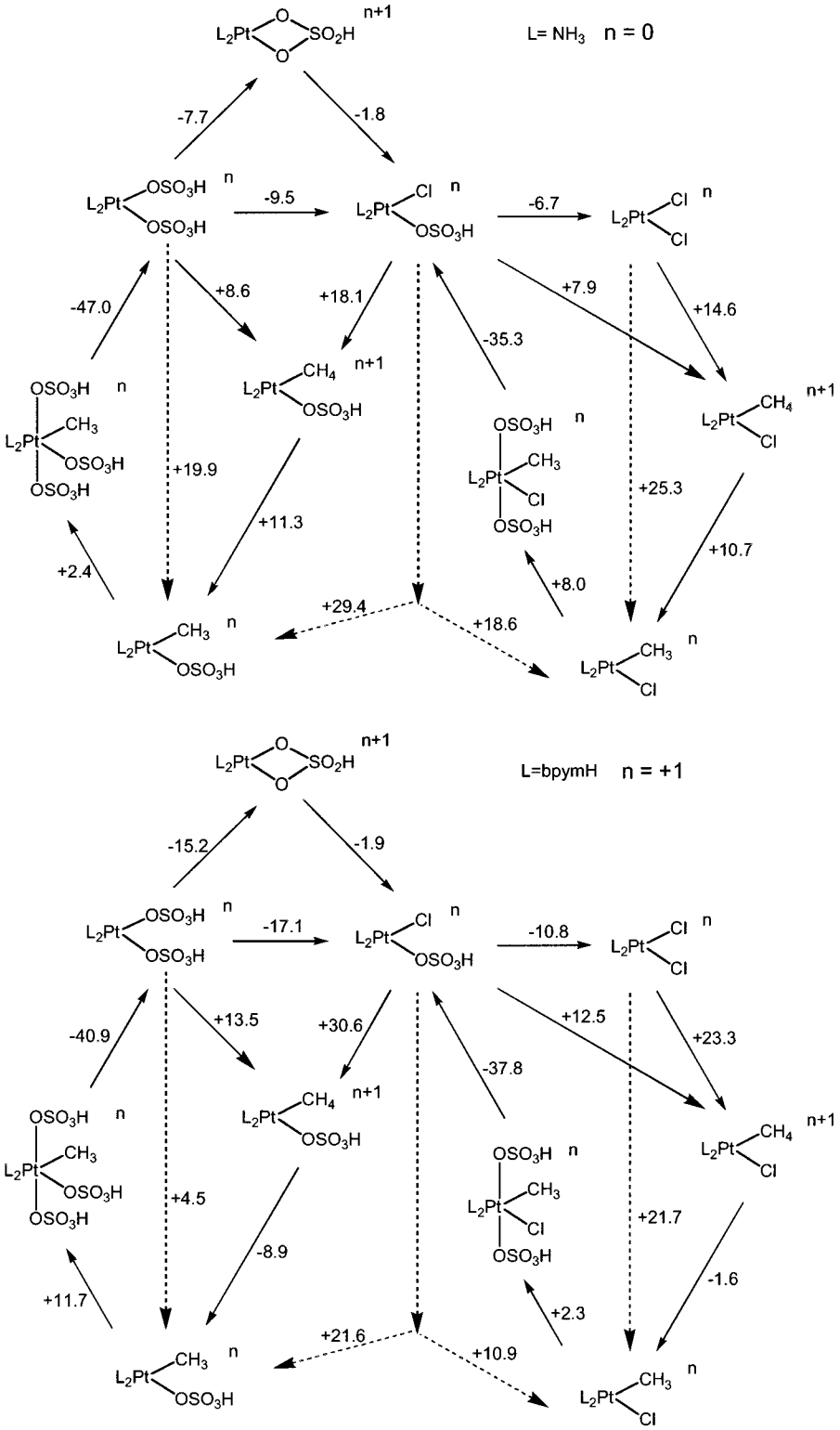

Figure 8. Calculated overall thermodynamics of the catalytic cycle: (a, top) energetics for the L = NH_3 case; (b, bottom) energetics for the L_2 = bpym case.

formation of the H−X bond. We have not been able to locate a transition state for such a single-step C−H activation.

4.3.2. Stable Species in Solution before Reacting with CH_4. Before reaction with methane, the most thermodynamically stable species in solution among the four species involved in reactions **6**−**9** is L_2PtCl_2 for all ligands, L. The least favored species is $L_2Pt(OSO_3H)_2$, with the exception of $(OSO_3H)_2Pt(\eta^2\text{-}OSO_3H)^-$. For L_2 = bpym, bpymH_2, η^2-OSO_3H, we find that $L_2Pt(\eta^2\text{-}OSO_3H)$ is slightly favored over $L_2Pt(Cl)(OSO_3H)$ in solution. However, the concentration of sulfuric acid (the solvent) is $\sim 10^4$ times greater than any of the other species in solution, suggesting that there is a small but non-negligible amount of $L_2Pt(Cl)(OSO_3H)$ and $L_2Pt(\eta^2\text{-}OSO_3H)$ in solution.

Table 2. Energetics of L_2PtXY Complexes

compd	electronic E (hartree)	solvation E (kcal/mol)	ZPE (kcal/mol)	$G_{0\rightarrow 453K}$ (kcal/mol)
(a) L = NH_3; $n = 0$				
$[L_2Pt(Cl)_2]^n$	−1 152.799 824	−30.3	51.4	−38.0
$[L_2Pt(Cl)(CH_4)]^{n+1}$	−732.838 042 4	−74.0	80.2	−39.5
$[L_2Pt(Cl)(CH_3)]^n$	−732.484 995 2	−23.1	72.8	−40.0
$[L_2Pt(Cl)(CH_3)(OSO_3H)_2]^n$	−2 131.755 517	−37.4	110.2	−57.0
$[L_2Pt(Cl)(OSO_3H)]^n$	−1 392.230 355	−37.4	68.8	−45.6
$[L_2Pt(OSO_3H)(CH_4)]^{n+1}$	−972.256 873	−84.8	97.0	−46.7
$[L_2Pt(OSO_3H)(CH_3)]^n$	−971.913 644 5	−32.3	90.2	−42.5
$[L_2Pt(OSO_3H)_3(CH_3)]^n$	−2 371.173 061	−41.8	128.1	−61.6
$[L_2Pt(OSO_3H)_2]^n$	−1 631.664 687	−42.0	86.8	−51.1
$[L_2Pt(\eta^2\text{-}OSO_3H)]^{n+1}$	−931.743 466 2	−82.0	68.2	−42.7
(b) L = OSO_3H; $n = -2$				
$[L_2Pt(Cl)_2]^n$	−2 439.049 954	−160.3	37.4	−51.2
$[L_2Pt(Cl)(CH_4)]^{n+1}$	−2 019.320 910	−49.7	66.3	−49.6
$[L_2Pt(Cl)(CH_3)]^n$	−2 018.739 748	−163.7	59.3	−54.2
$[L_2Pt(Cl)(CH_3)(OSO_3H)_2]^n$	−3 418.053 658	−143.4	96.0	−65.0
$[L_2Pt(Cl)(OSO_3H)]^n$	−2 678.500 690	−151.5	54.9	−56.1
$[L_2Pt(OSO_3H)(CH_4)]^{n+1}$	−2 258.741 620	−50.3	83.0	−58.0
$[L_2Pt(OSO_3H)(CH_3)]^n$	−2 258.195 206	−152.4	76.8	−58.1
$[L_2Pt(OSO_3H)_3(CH_3)]^n$	−3 657.493 744	−138.9	113.3	−70.7
$[L_2Pt(OSO_3H)_2]^n$	−2 917.943 707	−145.6	72.5	−60.9
$[L_2Pt(\eta^2\text{-}OSO_3H)]^{n+1}$	−2 218.222 290	−47.2	54.2	−51.9
(c) $L_2 = \eta^2$-OSO_3H; $n = -1$				
$[L_2Pt(Cl)_2]^n$	−1 739.356 347	−55.6	18.8	−42.4
$[L_2Pt(Cl)(CH_4)]^{n+1}$	−1 319.515 383	−13.1	47.7	−42.6
$[L_2Pt(Cl)(CH_3)]^n$	−1 319.062 922	−53.1	41.2	−43.9
$[L_2Pt(Cl)(CH_3)(OSO_3H)_2]^n$	−2 718.344 868	−52.3	78.1	−62.9
$[L_2Pt(Cl)(OSO_3H)]^n$	−1 978.793 194	−46.7	36.9	−46.3
$[L_2Pt(OSO_3H)(CH_4)]^{n+1}$	−1 558.928 694	−24.7	64.4	−49.3
$[L_2Pt(OSO_3H)(CH_3)]^n$	−1 558.492 265	−50.6	58.4	−49.8
$[L_2Pt(OSO_3H)_3(CH_3)]^n$	−2 957.777 913	−47.0	96.2	−67.0
$[L_2Pt(OSO_3H)_2]^n$	−2 218.222 290	−47.2	54.2	−51.9
$[L_2Pt(\eta^2\text{-}OSO_3H)]^{n+1}$	−1 518.423 676	−19.7	35.8	−44.4
(d) L_2 = bpymH$_2$; $n = +2$				
$[L_2Pt(Cl)_2]^n$	−1 567.650 889	−221.5	103.1	−46.5
$[L_2Pt(Cl)(CH_4)]^{n+1}$	−1 147.460 954	−396.6	131.3	−48.8
$[L_2Pt(Cl)(CH_3)]^n$	−1 147.363 169	−204.6	125.5	−48.6
$[L_2Pt(Cl)(CH_3)(OSO_3H)_2]^n$	−2 546.600 627	−210.7	161.6	−65.8
$[L_2Pt(Cl)(OSO_3H)]^n$	−1 807.066 587	−226.8	120.2	−54.9
$[L_2Pt(OSO_3H)(CH_4)]^{n+1}$	−1 386.878 566	−395.0	147.9	−56.8
$[L_2Pt(OSO_3H)(CH_3)]^n$	−1 386.777 249	−211.6	142.4	−54.6
$[L_2Pt(OSO_3H)_3(CH_3)]^n$	−2 786.041 018	−185.1	178.3	−71.1
$[L_2Pt(OSO_3H)_2]^n$	−2 046.479 393	−234.3	137.2	−59.3
$[L_2Pt(\eta^2\text{-}OSO_3H)]^{n+1}$	−1 346.383 048	−398.2	119.5	−51.1
(e) L_2 = bpymH; $n = +1$				
$[L_2Pt(Cl)_2]^n$	−1 567.468 698	−80.0	95.8	−45.9
$[L_2Pt(Cl)(CH_4)]^{n+1}$	−1 147.400 134	−181.2	124.2	−47.9
$[L_2Pt(Cl)(CH_3)]^n$	−1 147.168 266	−68.9	118.0	−47.2
$[L_2Pt(Cl)(CH_3)(OSO_3H)_2]^n$	−2 546.419 229	−80.9	154.7	−67.9
$[L_2Pt(Cl)(OSO_3H)]^n$	−1 806.888 369	−88.5	113.0	−54.6
$[L_2Pt(OSO_3H)(CH_4)]^{n+1}$	−1 386.815 271	−186.6	140.8	−54.7
$[L_2Pt(OSO_3H)(CH_3)]^n$	−1 386.582 419	−82.4	135.0	−54.2
$[L_2Pt(OSO_3H)_3(CH_3)]^n$	−2 785.826 856	−89.8	172.0	−74.5
$[L_2Pt(OSO_3H)_2]^n$	−2 046.307 444	−97.4	130.7	−57.4
$[L_2Pt(\eta^2\text{-}OSO_3H)]^{n+1}$	−1 346.316 248	−187.7	112.3	−50.4
(f) L_2 = bpym; $n = 0$				
$[L_2Pt(Cl)_2]^n$	−1 567.127 652	−23.7	87.6	−46.4
$[L_2Pt(Cl)(CH_4)]^{n+1}$	−1 147.174 537	−54.6	116.3	−48.1
$[L_2Pt(Cl)(CH_3)]^n$	−1 146.814 217	−18.2	109.7	−47.2
$[L_2Pt(Cl)(CH_3)(OSO_3H)_2]^n$	−2 546.068 763	−32.5	146.5	−68.0
$[L_2Pt(Cl)(OSO_3H)]^n$	−1 806.553 597	−30.4	104.8	−52.0
$[L_2Pt(OSO_3H)(CH_4)]^{n+1}$	−1 386.588 920	−67.0	133.2	−54.7
$[L_2Pt(OSO_3H)(CH_3)]^n$	−1 386.235 047	−27.2	126.5	−55.7
$[L_2Pt(OSO_3H)_3(CH_3)]^n$	−2 785.484 031	−37.5	164.3	−70.7
$[L_2Pt(OSO_3H)_2]^n$	−2 045.987 901	−33.5	122.8	−57.3
$[L_2Pt(\eta^2\text{-}OSO_3H)]^{n+1}$	−1 346.090 643	−63.1	104.1	−50.8
(g) L = Cl; $n = -2$				
$[L_2Pt(OSO_3H)(CH_4)]^{n+1}$	−1 779.884 681	−51.0	48.3	−47.2
$[L_2Pt(OSO_3H)(CH_3)]^n$	−1 779.271 180	−175.1	41.2	−45.1
$[L_2Pt(OSO_3H)_3(CH_3)]^n$	−3 178.602 004	−147.4	78.6	−60.9
$[L_2Pt(OSO_3H)_2]^n$	−2 439.049 954	−160.3	37.4	−51.2
$[L_2Pt(\eta^2\text{-}OSO_3H)]^{n+1}$	−1 739.356 347	−55.6	18.8	−42.4

Table 3. Reaction Thermodynamics of L_2PtXY (kcal/mol)

reacn	L = NH_3	L = OSO_3H	L_2 = OSO_3H	L_2 = bpymH$_2$	L_2 = bpymH	L_2 = bpym	L = Cl
(a) Enthalpies at 0 K (Solvation and ZPE Included)							
1a	17.1	25.4	27.6	28.2	26.2	24.3	
2a	10.5	−10.9	−17.0	−7.0	−2.9	1.4	
3a	−31.3	−24.7	−23.9	−3.7	−17.5	−21.9	
4a	−13.7	−4.0	8.7	−24.2	−18.0	−18.1	
5a	13.7	18.8	11.5	14.1	17.6	17.9	
10a	27.6	14.5	10.6	21.2	23.3	25.7	
11a	24.2	7.9	−5.6	7.1	14.7	19.3	
1b	20.1	34.2	20.5	33.5	31.6	25.6	
2b	6.5	−20.0	−12.7	−13.1	−10.1	0.6	−0.7
3b	−19.0	−22.0	−22.4	12.4	−8.4	−13.4	−27.1
4b	−24.3	−4.1	4.6	−39.7	−24.8	−28.0	−9.5
5b	16.0	25.4	9.8	19.8	22.6	20.1	16.6
10b	26.7	14.2	7.9	20.3	21.5	26.2	
11b	22.6	5.3	−2.9	6.6	12.5	20.7	15.8
6	−3.4	−6.6	−16.1	−14.1	−8.6	−6.4	
7	−4.1	−8.8	−10.8	−13.7	−9.0	−5.5	
8	13.8	27.0	4.6	0.8	7.7	9.2	15.6
9	−17.9	−35.9	−15.4	−14.5	−16.7	−14.7	
(b) Free Energy Corrections to 453 K (Solvation and ZPE Included)							
1a	14.6	26.0	26.5	24.9	23.3	21.7	
2a	10.7	−14.8	−17.7	−6.1	−1.6	2.9	
3a	−8.0	4.9	−2.5	19.4	2.3	−2.3	
4a	−35.3	−28.2	−7.8	−46.4	−37.8	−35.2	
5a	7.9	13.4	3.3	8.3	12.5	10.0	
10a	25.3	11.2	8.8	18.8	21.7	24.6	
11a	18.6	−1.4	−14.4	2.3	10.9	12.9	
1b	18.1	31.4	16.6	30.6	30.6	22.0	
2b	11.3	−19.5	−12.5	−10.2	−8.9	0.2	2.1
3b	2.4	5.8	0.8	36.2	11.7	12.0	−2.5
4b	−47.0	−27.4	−13.4	−61.0	−40.9	−47.7	−32.8
5b	8.6	16.5	0.4	10.4	13.5	10.8	8.6
10b	29.4	11.9	4.1	20.4	21.6	22.2	
11b	19.9	−3.0	−12.1	0.2	4.5	11.0	10.7
6	−6.7	−12.6	−23.2	−16.5	−10.8	−11.7	
7	−9.5	−14.9	−16.1	−20.2	−17.1	−11.2	
8	−7.7	6.2	−17.8	−21.0	−15.2	−14.3	−5.7
9	−1.8	−21.1	1.7	0.8	−1.9	3.1	

The exothermicity for reaction **6** ranges from −23.2 kcal/mol ($L_2 = \eta^2$-OSO_3H) to −6.7 kcal/mol ($L_2 = (NH_3)_2$) with the sequence

$$\eta^2\text{-}OSO_3H > bpymH_2 > (OSO_3H)_2 > bpym > bpymH > (NH_3)_2$$

The exothermicity for reactions **9** and **6** from most to least exothermic is

$$(OSO_3H)_2 > \eta^2\text{-}OSO_3H > bpymH_2 > bpymH > bpym \approx (NH_3)_2$$

with values ranging from −33.7 to −8.5 kcal/mol. Pt-(η^2-$OSO_3H)_2$ is particularly unfavorable.

4.3.3 Thermodynamics of C−H Activation. (a) Overall Thermodynamics to Form the CH_3 Complex. We consider L_2PtCl_2 first, since it is the most stable species in solution. The formation of $L_2Pt(Cl)(CH_3)$ from L_2PtCl_2 (reaction **10a**) is endothermic for all ligands. The bisulfate ligands are the least endothermic (+8.8 and +11.2 kcal/mol). The bpym ligands lead to +18.8, +21.7, and +24.6 kcal/mol as the number of protons on the bpym is decreased from 2 to 0. The L = NH_3 case is the most endothermic (+25.3 kcal/mol).

With $L_2Pt(Cl)(OSO_3H)$ as the starting material and going to $L_2Pt(Cl)(CH_3)$ (reaction **11a**, which combines **6** and **10a**), the L_2 = bisulfate and L_2 = (bisulfate)$_2$ cases are *exo*thermic (−1.4 and −14.4 kcal/mol). The trend (most exothermic first) is

$$\eta^2\text{-}OSO_3H > (OSO_3H)_2 > bpymH_2 > bpymH > bpym > (NH_3)_2$$

(b) Thermodynamics for Forming the CH_4 Complex. Since we find that the C−H activation step includes the formation of the methane complex $L_2Pt(Cl)(CH_4)$, it is relevant to consider the energetics for reaction **1a** by starting from L_2PtCl_2 (or **5a** starting from $L_2PtCl(OSO_3H)$). We find that reaction **1a** is least endothermic for NH_3 ligands, moderately endothermic for bpym ligands, and most endothermic for bisulfate ligands. Reaction **5a** shows a similar trend.

For ease in comparing the thermodynamics of several different ligands, we have chosen to consider that the Cl^- originally on the catalyst L_2PtCl_2 is dissociated completely to form HCl infinitely separated from the CH_4−Pt(II) complex as in eqs 14a and 14b

$$[L_2Pt^{II}Cl_2]^{m+} + CH_4 + H_2SO_4 \rightarrow [L_2Pt^{II}Cl(CH_4)]^{(m+1)+} + HCl + OSO_3H^- \quad (14a)$$

$$[L_2Pt^{II}Cl(CH_4)]^{(m+1)+} + OSO_3H^- \rightarrow [L_2Pt^{II}Cl(CH_3)]^{m+} + H_2SO_4 \quad (14b)$$

and corresponding to steps **1a** and **2a**. We do this despite the result that our calculations find the process of eqs 7a and 7b, in which the Cl^- stays associated with the CH_4−Pt(II) complex. The reason is that the calculations with weakly bound ligands are very difficult (particularly when OSO_3H is displaced as in **1b** and **2b**, where there are many very low lying vibrations complicating calculations for transition states). We expect the trends to be the same.

(c) L = NH_3 Case. Comparing the relative energetics of reactions **1a** and **10a** (and analogously reactions **5a** and **11a**), we find that, for the NH_3 ligands, formation of the $L_2Pt(Cl)(CH_4)$ complex is significantly less endothermic than forming $L_2Pt(Cl)(CH_3)$, +14.6 and +25.3 kcal/mol, leading to an endothermic step **2a** of +10.7 kcal/mol.

(d) L = OSO_3H Case. The above trend for L = NH_3 is reversed for the bisulfate ligands; reaction **2a** is −14.8 and −17.7 kcal/mol for two and one bisulfate ligands, respectively.

(e) L_2 = bpym Case. The bpym ligands lead to intermediate results. Reaction **2a** is exothermic (−6.1 kcal/mol) for $bpymH_2$ and increases in endothermicity with deprotonation (−1.6 and +2.9 for bpymH and bpym, respectively).

Our calculations investigating the kinetics of C−H activation for L_2 = bpym (section 4.2.1, Figure 6) find that the Cl^- remains associated with the complex in an ion pair (rather than separated at infinity as above). Here we find that the reaction corresponding to **2a** (**B** → **C**) is exothermic (ΔH(sol, 0 K)= −11.2 kcal/mol). The fact that no methane complex has been isolated experimentally suggests that the methane complex remains tightly associated as an ion pair. Thus, **A** → **B** → **C** in Figure 5 is a more correct description of the reaction than **1a** and **2a** in Figure 7b.

Among the bipyrimidine complexes, the singly protonated $[(bpymH)PtCl_2]^+$ is 4.9 kcal/mol more stable than the doubly protonated $[(bpymH_2)PtCl_2]^{2+}$. Thus, although the bpymH should be dominant, the $bpymH_2$ species will also be present in significant amounts. For L_2 = bpymH, reaction **10a** is endothermic by +21.7 kcal/mol, whereas for L_2 = $bpymH_2$, it is less endothermic (+18.8 kcal/mol). As a result, the doubly protonated complex $[(bpymH_2)Pt(Cl)(CH_3)]^{2+}$ is more stable (by 2.9 kcal/mol) than the singly protonated $[(bpymH)Pt(Cl)(CH_3)]^+$.

(f) OSO_3H Anion. The catalytic cycle on the left (reactions **1b**, **2b**, **5b**, **10b**, and **11b**) where X = OSO_3H shows trends similar to the cycle on the right (X = Cl). However, this cycle is thermodynamically less accessible, since reactions **6** and **7** are exothermic.

(g) Comparison with Calculations by Hush. In contrast with our results, Hush and co-workers[31] found that replacement of X = Cl with X = OSO_3H is thermodynamically favorable; hence, they examine reactions related to the left cycle of Figure 7b. For example, they calculated

$$[(NH_3)_2PtCl_2]^0 + H_2SO_4 + CH_4 \rightarrow [(NH_3)_2Pt(CH_3)(OSO_3H)]^0 + 2\ HCl \quad (15)$$

(this corresponds to reaction **10b** minus reaction **6**) to be exothermic (ΔH_{0K} = −6.2 kcal/mol). In contrast, we find this reaction to be quite endothermic (ΔH_{0K} = +30.0 kcal/mol). This large discrepancy is due mainly to the relative solvation energies of the two Pt complexes. We find that the solvation energies of $[(NH_3)_2PtCl_2]^0$ and $[(NH_3)_2Pt(CH_3)(OSO_3H)]^0$ are close in energy (−30.3 and −32.3 kcal/mol, respectively), whereas Hush calculated a large difference (−9.5 and −50.4 kcal/mol, respectively).

4.3.4. Thermodynamics of Oxidation. The oxidation step (reaction **3a**) involves a two-electron-redox reaction: oxidation of Pt(II) to Pt(IV) coupled to reduction of S(VI) in the form of SO_3 to S(IV) in the form of SO_2 (eq 8). Experimentally, the oxidation step is rate-determining. We find that formation of the Pt(IV) octahedral complex is most exothermic for the NH_3 ligand (−8.0 kcal/mol). It is mildly exothermic (−2.5 kcal/mol) for the η^2-OSO_3H ligand. For the bpym ligands, this step is +19.4 kcal/mol for the doubly protonated form, 2.3 kcal/mol for the singly protonated form, and −2.3 for the unprotonated form. Assuming that the activation barrier to oxidation follows the same trend, we would expect that the NH_3 ligand complex should have the lowest barriers and hence be the most active (as observed).

The analogous reaction on the left side of the catalytic cycle (reaction **3b**) follows the same general trend (comparing the different ligands), except that all these reactions are significantly more endothermic than the reaction **3a**. Thus, we conclude that retention of one Cl^- leads to the most active form of the catalyst. This is in good agreement with experimental evidence that Cl is important for the oxidation step. When the $L_2Pt(OSO_3H)_2$

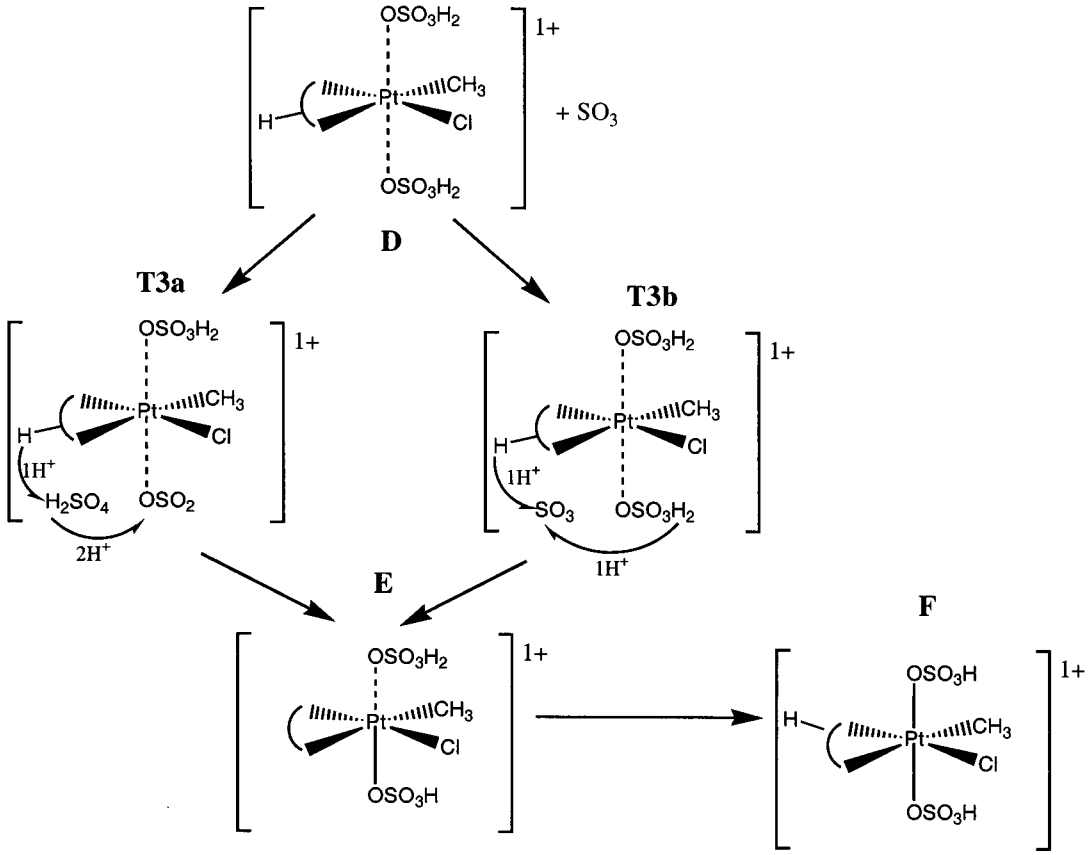

Figure 9. Suggested mechanism for the oxidation step.

complex was used as the starting material instead of L_2PtCl_2, the activity was drastically reduced.[38]

On the basis of preliminary calculations of the intermediates involved in the oxidation step, our suggested mechanism for oxidation is shown in Figure 9, illustrated with L_2 = bpymH. Structure **D** is the Pt(II)−CH_3 intermediate with two additional H_2SO_4 solvent molecules loosely associated with the axial positions. Since oxidation of Pt(II) to Pt(IV) requires the simultaneous reduction of SO_3 to SO_2, we have added one SO_3 molecule to the system. SO_3 may displace one of the axial H_2SO_4 molecules, the latter moving to a position that bridges the proton of the bpym ligand and SO_3. The bpym ligand rotates slightly and one proton points toward the bridging H_2SO_4 molecule to form a hydrogen-bonding network (see Figure 10). Simultaneous proton transfer across this bridge (concurrent with electron transfer from Pt to SO_3) can take place to transform SO_3 to reduced H_2SO_3 (illustrated by **T3a**). H_2SO_3 goes into solution, favorably dissociating into SO_2 and H_2O. The remaining bisulfate ion can form a strong Pt−O bond (∼2 Å), giving rise to structure **E**. Subsequent proton transfer in solution leads to structure **F**.

An alternate route (illustrated by **T3b**) keeps the H_2SO_4 molecules associated with the axial positions of the complex and utilizes SO_3 as the bridge. As before, to form H_2SO_3, one proton leaves the bpymH ligand and the other comes from the axial H_2SO_4 molecule. This route also leads to structures **E** and **F**.

The key to the oxidation step, therefore, is to transfer two protons and two electrons from the Pt(II) complex

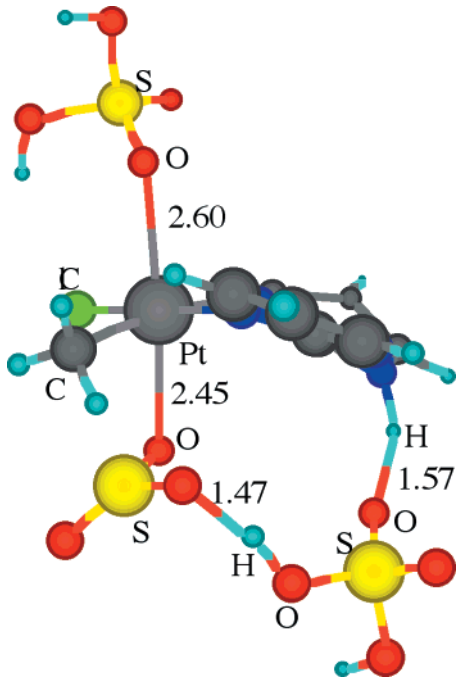

Figure 10. Structure of $[(bpymH_2)Pt(Cl)(CH_3)\cdots(SO_3)(H_2SO_4)_2]^{2+}$ involved in Figure 9.

to an SO_3 molecule, leading to the oxidized Pt(IV) complex. Formally, **D** has a bpymH (+1), a chloride (−1), and a bisulfate (−1) ligand. Since the net overall charge of the complex is +1, this leads to Pt(II). On the other hand, **E** formally has a bpym (0), a chloride (−1), and two bisulfate (−1 each) ligands. Since the net overall

(38) Periana, R. A. Unpublished results.

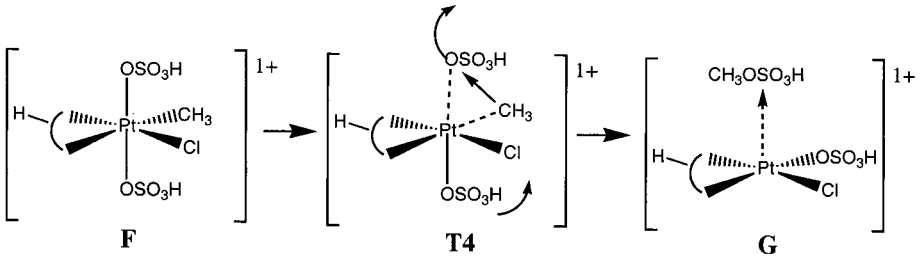

Figure 11. Suggested mechanism for the functionalization step.

charge of the complex is still +1, this leads to Pt(IV). Proton transfer from **E** to **F** reduces the net charge; hence, F is still formally Pt(IV).

4.3.5. Thermodynamics of Functionalization. The functionalization step involves removal of CH_3OSO_3H from the Pt(IV) complex via reductive elimination to regenerate a Pt(II) complex (eq 9). We find this step (reaction **4a**) to be exothermic for all ligands considered. Experimental evidence suggests that this is a fast step.[12] Methanol is then formed from the hydrolysis of CH_3OSO_3H, regenerating H_2SO_4.

$$CH_3OSO_3H + H_2O \rightarrow CH_3OH + H_2SO_4 \quad (16)$$

Preliminary calculations suggest (see Figure 11) that a key step is that a bisulfate ligand in the axial position (down in Figure 11) rotates toward the equatorial position, while the equatorial methyl is transferred to the other axial bisulfate (up in Figure 11). A detailed mechanistic study is in progress to delineate whether the CH_3OSO_3H formation is more favorable via S_N2 or a concerted three-center transition state.

5. Discussion

We find that critical to stability of the catalytic complex in concentrated sulfuric acid is having a ligand that in its protonated state (at low pH) still can bind strongly to the Pt center. The bipyrimidine ligand (doubly protonated in solution) still has two N centers to bind to the complex. Simple ammines would not live long in acidic media, since it is quite favorable for them to form free RNH_2^+ in solution, and the loss of the ammine ligands will eventually lead to the $PtCl_2$ precipitate and catalyst death. We expect that the favorable ligands should have at least three N π-acid sites with two nitrogens in the right positions to act as a bidentate ligand to the Pt complex plus at least one additional N to be protonated in sulfuric acid.

We find the oxidation step is most favorable for the ammine ligand. Since the oxidation step is rate-determining, this suggests that the ammine form of the catalyst should be responsible for the short-lived higher catalytic activity before precipitation occurs.

Although L_2PtCl_2 is the starting catalyst, our mechanism suggests that the first turnover leads to one Cl^- irreversibly lost as HCl. After the functionalization step, $L_2Pt(Cl)(OSO_3H)$ is regenerated. This becomes the starting point for subsequent catalytic cycles, which we find to have a lower barrier for the CH activation step.

We find that weaker binding L ligands enhance C−H activation by stabilizing the formation of a stronger Pt−C bond in the Pt(II)−CH_3 intermediate. We calculate the enthalpy of C−H activation to be less endothermic for the weaker binding O-based bisulfate ligands than for the N-based ligands (reactions **10** and **11** in Table 3a).

As discussed in section 4.2.1, the methane ion-pair intermediate complex leads to calculated relative activation barriers for conversion to CH_3 versus loss of CH_4 that are in good agreement with H/D exchange experiments (for bpym). Our calculations also suggest that the reaction pathway involving the close association of X^- (X = Cl, OSO_3H) keeps the intermediate methane complex reactive to forming the Pt(II)−CH_3 species.

We find that C−H activation using (bpym)$PtCl_2$ proceeds more favorably via electrophilic substitution, whereas $(NH_3)_2PtCl_2$ favors oxidative addition.

We find that decreasing protonation of bpym favors a more rapid oxidation step. This is reasonable, since the less positive ligand would stabilize the Pt(IV) complex. Hence, we expect that having too many protonation sites on L may destabilize the oxidation complex. In addition, we expect that, as the solvent is made less acidic, the oxidation step should be increasingly favorable. Our calculations make it clear that step **3a** is much more favorable than **3b**: i.e., retention of one Cl^- ligand leads to the most active form of the catalyst.

Although water is involved in the hydrolysis to convert methyl bisulfate to methanol (see eq 16), the presence of water in the catalytic cycle has deleterious effects on activity. As more water is generated from the decomposition of H_2SO_3 to SO_2 and H_2O (byproduct of the oxidation step), the equilibrium of H_2SO_4 and SO_3 (direct oxidant) shifts to reduce the concentration of SO_3 and, hence, inhibit the oxidation step. Preliminary calculations also suggest that water can bind to the axial positions to block the oxidation step or compete with methane at the equatorial position to block C−H activation.

6. Conclusions

Modern DFT methods with solvation can be useful in elucidating reaction mechanisms, even for reactions in very acidic media. Our studies suggest that in order to prevent catalyst death via precipitation of $PtCl_2$ under highly concentrated acidic conditions, suitable ligands require multiple protonation sites. The protonated free ligand should have open electron donor sites to form a complex with $PtCl_2$. This explains the observed stability of the bipyrimidine catalyst, which does not favorably undergo ligand exchange with bisulfate. In contrast, the ammine catalyst favorably undergoes ligand exchange to form the bisulfate complex in sulfuric

acid, which will eventually lead to $PtCl_2$ precipitation and catalyst death.

We calculate the thermodynamics of the C−H activation step to be most favorable for the weaker-binding bisulfate ligands. We find that the activation proceeds through a methane complex rather than the 14-electron T-complex. Our calculated relative barriers for a two-step C−H activation mechanism are in good agreement with observed experimental isotope results. We find that the thermodynamics of the rate-determining oxidation step is most favorable for the ammine ligand, suggesting that the ammine form of the catalyst should be responsible for the short-lived higher catalytic activity before precipitation of $PtCl_2$ occurs. This is in good agreement with the experimentally observed higher activity of the ammine catalyst over the bipyrimidine catalyst.

Acknowledgment. This research was initiated with funding from BP and the NSF (Grant No. CHE 95-22179) and completed with funding from Chevron. We thank Dr. Bill Schinski, Dr. Yongchun Tang, and Dr. Dean Philipp for helpful suggestions. The facilities of the MSC are also supported by grants from DOE-ASCI, ARO/DURIP, ARO/MURI, Beckman Institute, Seiko-Epson, 3M, Avery-Dennison, Dow, Kellogg's, and Asahi Chemical.

OM0101691